Density profiles of Ar adsorbed in slits of CO_2: Spontaneous symmetry breaking revisited

Leszek Szybisz[1,2,3,a)] and Salvador A. Sartarelli[4]
[1]*Laboratorio TANDAR, Departamento de Física, Comisión Nacional de Energía Atómica, Av. del Libertador 8250, RA-1429 Buenos Aires, Argentina*
[2]*Departamento de Física, Facultad de Ciencias Exactas y Naturales, Universidad de Buenos Aires, Ciudad Universitaria, RA-1428 Buenos Aires, Argentina*
[3]*Consejo Nacional de Investigaciones Científicas y Técnicas, Av. Rivadavia 1917, RA-1033 Buenos Aires, Argentina*
[4]*Instituto de Desarrollo Humano, Universidad Nacional de General Sarmiento, Gutierrez 1150, RA-1663 San Miguel, Argentina*

(Received 17 July 2007; accepted 19 February 2008; published online 24 March 2008)

A recently reported symmetry breaking of density profiles of fluid argon confined by two parallel solid walls of carbon dioxide is studied. The calculations are performed in the framework of a nonlocal density functional theory. It is shown that the existence of such asymmetrical solutions is restricted to a special choice for the adsorption potential, where the attraction of the solid-fluid interaction is reduced by the introduction of a hard-wall repulsion. The behavior as a function of the slit's width is also discussed. All the results are placed in the context of the current knowledge on this matter. © *2008 American Institute of Physics*. [DOI: 10.1063/1.2895747]

I. INTRODUCTION

In a quite recent paper, Berim and Ruckenstein[1] have reported symmetry breaking of the density profile of fluid argon (Ar) confined in a planar slit with identical walls of carbon dioxide (CO_2). These authors claimed that a completely symmetric integral equation provides an asymmetric profile which has a lower free energy than that of the lowest symmetric solution leading to a symmetry breaking phenomenon. It was assumed that the Ar atoms interact via a standard Lennard–Jones (LJ) potential characterized by the strength ε_{ff} and the atomic diameter σ_{ff}. The presented results were obtained from calculations carried out with the smoothed density approximation (SDA) version[2,3] of the nonlocal density functional theory (DFT) in the case of a closed planar slit with an effective width of $15\sigma_{ff}$. The symmetry breaking was found for temperatures between the experimental triple point for Ar, $T_t=83.8$ K, and a critical value $T_{sb}=106$ K. At each temperature, it was determined a range of average densities $\rho_{sb1}\leqslant\rho_{av}\leqslant\rho_{sb2}$ where the symmetry breaking occurs, outside this range a symmetric profile has the lowest free energy.

As a matter of fact, the adsorption of fluid Ar on a solid substrate of CO_2 was intensively studied for several decades (see, e.g., Refs. 4 and 5). In 1977 Ebner and Saam[6] analyzed phase transitions by assuming that atoms of the fluid interact with the solid wall via a 9-3 van der Walls potential (from here on denoted as ES potential) obtained from the assumption that Ar atoms interact with CO_2 molecules via a LJ interaction with parameters ε_{sf} and σ_{sf}. After this pioneering work, a large amount of work has been devoted to study this system with different numerical and analytical techniques. The attention was focused to analyze features such as the oscillatory behavior of the density profile which leads to a layered structure in the neighborhood of the flat substrate, the thin- to thick-film transitions, and wetting properties and prewetting jumps.[7–22] Berim and Ruckenstein[1] have also adopted the ES potential, however, a hard-wall repulsion was introduced in their calculations. In practice, such a hard wall diminishes the strength of the solid-fluid interaction.

The investigation of symmetry breaking in physical systems is a very exciting issue. This is due to the fact that such a feature may have fundamental theoretical implications. In many fields of physics the discovery of symmetry breaking leads to significant advances in the theory. Therefore it is important to place the results of Ref. 1 in the context of the current knowledge about adsorption into planar slits.

Asymmetric solutions for fluids confined in slits have been previously reported in the literature. About 20 years ago a Dutch Collaboration has carried out calculations on the Delft Molecular Dynamics Processor (DMDP), which was specially designed for molecular dynamics (MD) simulations of simple fluids.[23,24] The results were published in a series of papers by Sikkenk *et al.*[25,26] and Nijmeijer *et al.*[27,28] The simulations were performed for a canonical ensemble with two types of particles, 2904 of one type for building a solid substrate and several thousand of the other type for composing the fluid adsorbate. The temperature of the system was kept at $T^*=k_BT/\varepsilon_{ff}=0.9$ which is in between the fluid's triple-point temperature $T_t^*\simeq 0.7$ and the critical temperature $T_c^*\simeq 1.3$. The width of the slit was taken as $L=29.1\sigma_{ff}$, supposing that this distance be enough large to avoid any capillary effect. Such a system can support solid-liquid (SL), solid-vapor (SV), and liquid-vapor (LV) interfaces. These authors have studied wetting at LV coexistence by varying over a wide range the relative strength of the solid-fluid and fluid-fluid interactions defined by the ratio $\varepsilon_r=\varepsilon_{sf}/\varepsilon_{ff}$ of the LJ

a)Electronic mail: leszybisz@yahoo.com.ar.

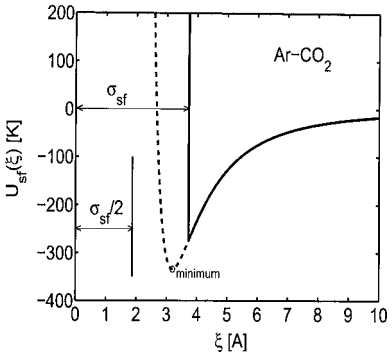

FIG. 1. Adsorption potential as a function of the distance from the real wall. The solid curve is the potential of Berim and Ruckenstein close to the left wall given by Eq. (2.23), while the dashed curve is that of Nilson and Griffiths given by Eq. (2.25).

parameters. The length scale of this interaction was taken as $\sigma_{sf}=0.941\sigma_{ff}$. For increasing ε_r from $\varepsilon_r \simeq 0.1$ toward $\varepsilon_r \simeq 1.0$ three cases were observed in Ref. 28.

(i) At low ε_r, *symmetric* profiles consisting of two SV interfaces and two LV interfaces are obtained, this situation corresponds to a complete wall drying as can be seen in Fig. 1 therein.

(ii) At intermediate ε_r, *asymmetric* profiles consisting of a SL, a LV, and a SV interface are obtained, here the wall attraction is sufficiently strong to produce a partial wetting, i.e., to support a rather thick film on one wall while a SV interface is present near the other wall, this feature is shown in Fig. 2 therein.

(iii) For the largest ε_r, symmetric profiles consisting of two SL interfaces and two LV interfaces are obtained, now the strength is enough to wet both walls, as can be seen in Fig. 3 therein.

The structure of the profiles mentioned above depends on the balance of the involved surface tensions γ_{SL}, γ_{LV}, and γ_{SV} which are related by Young's law [see, e.g., Eq. (2.1) in Ref. 29],

$$\gamma_{SV} = \gamma_{SL} + \gamma_{LV} \cos\,\theta, \tag{1.1}$$

where θ is the contact angle. The latter quantity is defined as the angle between the wall and the interface between the

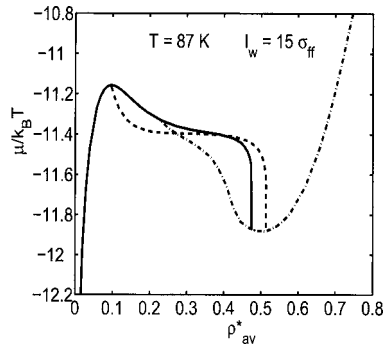

FIG. 2. Lagrange multiplier μ as a function of average density. The solid curves are results for symmetric film solutions. The dashed curve stands for values of asymmetric film solutions which occur in the range $\rho^*_{sb1} \leqslant \rho^*_{av} \leqslant \rho^*_{sb2}$. The dotted-dashed curve corresponds to drying-CC-like solutions.

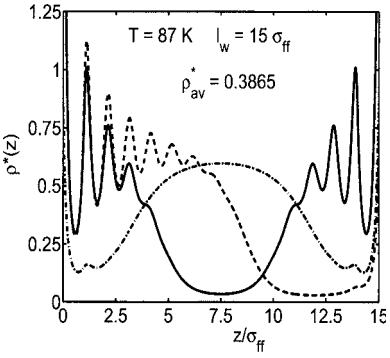

FIG. 3. Solutions of the EL Eq. (2.14) for the average density $\rho^*_{av}=0.3865$. The solid curve corresponds to the lowest symmetric solution, the dashed to the asymmetric one, and the dashed-dotted to the drying-CC-like one.

liquid and the vapor (see Fig. 1 in Ref. 29). The transition from (i) to (ii) takes place at the drying point $\theta=\pi$, whereas the transition from (ii) to (iii) takes place at the wetting point $\theta=0$.

It is worth noticing that Velasco and Tarazona[30] have carried out calculations in the framework of the SDA obtaining density profiles with the same structure to that reported in Refs. 25–28. The reader may look at Ref. 31 for a further comparison between MD and DFT results.

It is the aim of the present work to acquire a more accurate picture of the symmetry breaking reported in Ref. 1. In doing so, we explore size effects by comparing the results obtained for slits of widths $15\sigma_{ff}$ and $30\sigma_{ff}$. Next, we investigate the existence of stable asymmetric solutions for the density profiles when the position of the hard-wall repulsion introduced in Ref. 1 is changed. When the location of this hard wall is moved, the strength of the adsorption potential is varied, allowing a connection to the studies described in Refs. 25–28, 30, and 31. Several properties of the obtained solutions are discussed.

The paper is organized as follows. In Sec. II we provide a summary of the formalism underlying the present calculations. Special attention is devoted to the adsorption potential. The results and its analysis are reported in Sec. III. Final remarks are given in Sec. IV.

II. THE MODEL

The properties of a fluid adsorbed by an inert solid substrate may be studied by analyzing the grand free energy,[32]

$$\Omega = F - \mu N, \tag{2.1}$$

where F is the Helmholtz free energy, μ the chemical potential, and N the number of particles of the adsorbate,

$$N = \int \rho(\mathbf{r}) d\mathbf{r}. \tag{2.2}$$

Quantity F contains the energy due to the interaction between fluid atoms as well as the energy provided by the confining potential. In a DFT it is expressed in terms of the density profile $\rho(\mathbf{r})$,

$$F[\rho(\mathbf{r})] = F_{\text{int}}[\rho(\mathbf{r})] + \int d\mathbf{r}\rho(\mathbf{r})U_{sf}(\mathbf{r}). \tag{2.3}$$

Here $F_{\text{int}}[\rho(\mathbf{r})]$ is the intrinsic Helmholtz free energy functional and $U_{sf}(\mathbf{r})$ is the external potential produced by the slit's walls.

This formulation is usually applied to systems described by the grand canonical ensemble, i.e., at constant volume V, temperature T, and chemical potential μ. Such a situation corresponds to an open system in contact with reservoir which fixes T and μ. A minimization of Ω with respect to $\rho(\mathbf{r})$ leads to the Euler–Lagrange equation for the density profile and the number of particles may be evaluated with Eq. (2.2). For a closed system, i.e., a canonical ensemble with fixed N, one should treat μ as an unknown Lagrange multiplier to be determined from the minimization procedure.

A. DFT

Let us now summarize the DFT adopted for $F_{\text{int}}[\rho(\mathbf{r})]$. In the case of inhomogeneous classical fluids at temperature T the intrinsic free energy functional is decomposed into two kind of contributions.

(i) The ideal gas term $F_{\text{id}}[\rho(\mathbf{r})]$, which is given by the exact expression

$$F_{\text{id}}[\rho(\mathbf{r})] = k_BT\int d\mathbf{r}\rho(\mathbf{r})f_{\text{id}}[(\rho)] = k_BT\int d\mathbf{r}\rho(\mathbf{r})\{\ln[\Lambda^3\rho(\mathbf{r})] - 1\}, \tag{2.4}$$

with $\Lambda = \sqrt{2\pi\hbar^2/mk_BT}$ being the thermal de Broglie wavelength of a molecule of mass m.

(ii) The excess term $F_{\text{ex}}[\rho(\mathbf{r})]$, which accounts for the interparticle interactions, is a unique but unknown functional of the local density. For fluids with attractive interactions as the LJ one, the free energy is decomposed into the repulsive and attractive contributions. The repulsive interactions are then approximated by a hard-sphere functional with a certain choice of the hard-sphere diameter d_{HS},

$$F_{\text{HS}}[\rho(\mathbf{r})] = \int d\mathbf{r}\rho(\mathbf{r})f_{\text{HS}}[\bar{\rho}(\mathbf{r});d_{\text{HS}}], \tag{2.5}$$

whereas the attractive interactions are treated in most cases in a mean field fashion,

$$F_{\text{attr}}[\rho(\mathbf{r})] = \frac{1}{2}\int\int d\mathbf{r}d\mathbf{r}'\rho(\mathbf{r})\rho(\mathbf{r}')\Phi_{\text{attr}}(|\mathbf{r}-\mathbf{r}'|). \tag{2.6}$$

Here $\Phi_{\text{attr}}(r=|\mathbf{r}-\mathbf{r}'|)$ is the attractive part of the LJ potential.

In summary, the intrinsic Helmholtz free energy functional may be expressed as

$$F_{\text{int}}[\rho(\mathbf{r})] = F_{\text{id}}[\rho(\mathbf{r})] + F_{\text{ex}}[\rho(\mathbf{r})] = F_{\text{id}}[\rho(\mathbf{r})] + F_{\text{HS}}[\rho(\mathbf{r})] + F_{\text{attr}}[\rho(\mathbf{r})]. \tag{2.7}$$

The free energy functional for hard spheres plays a central role in DFT. Expressions for $f_{\text{HS}}[\bar{\rho}(\mathbf{r});d_{\text{HS}}]$ may be taken from the Percus–Yevick[33] or Carnahan–Starling[34] (CS) approximations for the equation of state of a uniform nonattractive hard-sphere fluid (see, e.g., Ref. 35). In a nonlocal DFT this quantity is evaluated as a function of a conveniently averaged density $\bar{\rho}(\mathbf{r})$.

For the calculations performed in the present work, we used the same SDA formalism adopted in the paper of Berim and Ruckenstein.[1] In this approach developed by Tarazona,[2,3] the excess of free energy density of hard spheres is written according to the semiempirical quasiexact CS expression,

$$f_{\text{HS}}[\bar{\rho}(\mathbf{r});d_{\text{HS}}] = f_{\text{CS}}[\bar{\eta}] = k_BT\left[\frac{\bar{\eta}(4-3\bar{\eta})}{(1-\bar{\eta})^2}\right]. \tag{2.8}$$

Here $\bar{\eta}=\bar{\rho}(\mathbf{r})V_{\text{HS}}$ is the packing fraction, where the factor $V_{\text{HS}}=\pi d_{\text{HS}}^3/6$ is the volume of a hard sphere. The smoothed density $\bar{\rho}(\mathbf{r})$ is defined as

$$\bar{\rho}(\mathbf{r}) = \int d\mathbf{r}\rho(\mathbf{r})w[|\mathbf{r}-\mathbf{r}'|;\bar{\rho}(\mathbf{r})], \tag{2.9}$$

with the following weighting function:

$$w[|\mathbf{r}-\mathbf{r}'|;\bar{\rho}(\mathbf{r})] = w_0[|\mathbf{r}-\mathbf{r}'|] + w_1[|\mathbf{r}-\mathbf{r}'|]\bar{\rho}(\mathbf{r}) + w_2[|\mathbf{r}-\mathbf{r}'|]\bar{\rho}^2(\mathbf{r}). \tag{2.10}$$

The expansion coefficients $w_0(r)$, $w_1(r)$, and $w_2(r)$ are density independent and its expressions as a function of $r=|\mathbf{r}-\mathbf{r}'|$ are given in the Appendix of Ref. 3.

To account for the fluid-fluid interaction we adopted, as in Ref. 1, the spherically symmetric LJ potential given in Eq. (2) of Ref. 8,

$$\Phi_{\text{attr}}(r) = \begin{cases} 4\varepsilon_{ff}\left[\left(\frac{\sigma_{ff}}{r}\right)^{12} - \left(\frac{\sigma_{ff}}{r}\right)^{6}\right] & \text{if } r \geqslant \sigma_{ff} \\ 0 & \text{if } r < \sigma_{ff}, \end{cases} \tag{2.11}$$

where σ_{ff} is the hard-core diameter of the fluid. The authors of Ref. 8 have used this LJ version just for studying the adsorption of Ar on CO_2, and it has been also utilized in several subsequent works on this system. The values of the interaction parameters for Ar are $\varepsilon_{ff}/k_B=119.76$ K and $\sigma_{ff}=3.405$ Å.

B. The Euler–Lagrange equation

The equilibrium density profile $\rho(\mathbf{r})$ of the fluid adsorbed in a closed slit is determined by a minimization of the free energy with respect to density variations with the constraint of a fixed number of particles N,

$$\frac{\delta}{\delta\rho(\mathbf{r})}\left[F_{\text{int}}[\rho(\mathbf{r})]+\int d\mathbf{r}'\rho(\mathbf{r}')[U_{sf}(\mathbf{r}')-\mu]\right]=0. \tag{2.12}$$

Here, i.e., for an ensemble with fixed V, T, and N, the Lagrange multiplier μ is an unknown quantity which should be determined from the constraint. It plays a role of a chemical potential but off the liquid-vapor coexistence conditions. Hence, it is not necessarily equal to μ_{coex} of an open slit in equilibrium with a reservoir at temperature T (see, e.g., Ref. 36).

In the case of a planar symmetry where the flat walls exhibit an infinite extent in the x and y directions, the profile depends only of the coordinate z perpendicular to the substrate. For this geometry the variation of Eq. (2.12) yields the following Euler–Lagrange (EL) equation,

$$\frac{\delta F}{\delta\rho(z)}+U_{sf}(z)=\frac{\delta[F_{\text{id}}+F_{\text{HS}}]}{\delta\rho(z)}+\int dz'\rho(z')\bar{\Phi}_{\text{attr}}(|z-z'|)+U_{sf}(z)=\mu. \tag{2.13}$$

For a slit of effective width ℓ_w this EL equation may be cast into the form

$$k_BT\ln[\Lambda^3\rho(z)]+Q(z)=\mu, \tag{2.14}$$

where

$$Q(z)=k_BT\frac{4\bar{\eta}(z)-3\bar{\eta}^2(z)}{[1-\bar{\eta}(z)]^2}+k_BT\frac{\pi d_{\text{HS}}^3}{6}\int_0^{\ell_w}dz'\rho(z')\frac{4-2\bar{\eta}(z')}{[1-\bar{\eta}(z')]^3}\frac{\delta\bar{\rho}(z')}{\delta\rho(z)}+\int_0^{\ell_w}dz'\rho(z')\bar{\Phi}_{\text{attr}}(|z-z'|)+U_{sf}(z). \tag{2.15}$$

The number of particles per unit area of one wall of the slit is

$$N_s=\int_0^{\ell_w}\rho(z)dz. \tag{2.16}$$

In order to get solutions for $\rho(z)$ it is useful to rewrite Eq. (2.14) as

$$\rho(z)=\rho_0\exp\left(-\frac{Q(z)}{k_BT}\right), \tag{2.17}$$

with

$$\rho_0=\frac{1}{\Lambda^3}\exp\left(\frac{\mu}{k_BT}\right). \tag{2.18}$$

The relation between μ and N_s is obtained by substituting Eq. (2.17) into the constraint given by Eq. (2.16),

$$\mu=-k_BT\ln\left[\frac{1}{N_s\Lambda^3}\int_0^{\ell_w}dz\exp\left(-\frac{Q(z)}{k_BT}\right)\right]. \tag{2.19}$$

For the calculations carried out in the present work we set $d_{\text{HS}}=\sigma_{ff}$ as it was done in Ref. 1.

The asymmetry of the density profiles is measured by the parameter

$$\Delta_N=\frac{1}{2N_s}\int_0^{\ell_w}dz|\rho(z)-\rho(\ell_w-z)|. \tag{2.20}$$

According to this definition, if the profile is completely asymmetrical about the middle of the slit [$\rho(z<\ell_w/2)\neq 0$ and $\rho(z\geqslant\ell_w/2)=0$] this parameter becomes unity, while for symmetric solutions it vanishes.

C. Adsorption potential

The model van der Waals (9-3) potential proposed by Ebner and Saam,[6] i.e. the ES potential, is

$$U_{sf}(z)=\begin{cases}\frac{2\pi}{3}\epsilon_{\text{eff}}\left[\frac{2}{15}\left(\frac{\sigma_{sf}}{z}\right)^9-\left(\frac{\sigma_{sf}}{z}\right)^3\right] & \text{if } z>0\\ 0 & \text{if } z\leqslant 0,\end{cases} \tag{2.21}$$

with $\epsilon_{\text{eff}}=\varepsilon_{sf}\rho_s\sigma_{sf}^3$ being the effective strength, was adopted for almost all the abovementioned studies of the adsorption of Ar atoms on a flat wall of solid CO_2. The exception is the experimental and theoretical investigation performed by Mistura *et al.*,[22] where a more realistic adsorption potential calculated on the basis an *ab initio* expansion of Marshall *et al.*[37] was used. The ES expression is obtained when one assumes that Ar atoms interact with CO_2 atoms via a LJ (12-6) potential and subsequently integrates this potential over a continuum of CO_2 substrate atoms with a reduced density $\rho_s^*=\rho_s\sigma_{sf}^3=0.988$. The cross parameters of the potential are determined by using the Lorentz–Berthelot rules. So that, the van der Waals strength ε_{sf} is the square root of the product of the argon and CO_2 van der Waals strengths, while the hard-core diameter σ_{sf} is the mean of the argon and CO_2 hard-core diameters, while the parameters evaluated in this way are $\varepsilon_{sf}/k_B=153$ K and $\sigma_{sf}=3.727$ Å.

Berim and Ruckenstein[1] have investigated the Ar–CO_2 system utilizing, in principle, the ES potential. However, by looking at their paper one realizes that according to Eq. (A5) of the Appendix

$$U_{sf1}(z)=\frac{2\pi}{3}\epsilon_{\text{eff}}\left[\frac{2}{15}\left(\frac{\sigma_{sf}}{z+\sigma_{sf}}\right)^9-\left(\frac{\sigma_{sf}}{z+\sigma_{sf}}\right)^3\right], \tag{2.22}$$

which accounts for the solid-fluid interaction at one of the walls, a hard-wall repulsion was located at a distance σ_{sf} from the real wall of the slit. In agreement with this assumption, the total confining potential exerted on Ar atoms by the two walls separated by a distance L was expressed as

$$U_{sf}(z)=U_{sf1}(z+\sigma_{sf})+U_{sf2}(\ell_w-z+\sigma_{sf}). \tag{2.23}$$

Here the effective width of the slit is

$$\ell_w=L-2\sigma_{sf}. \tag{2.24}$$

This scenario is depicted in Fig. 2 of Ref. 1. In this context, it is interesting to notice that Nilson and Griffiths[38] in order to study the adsorption of a fluid in a planar slit have written in their Eq. (10) the total fluid-solid potential as

TABLE I. Values of the Helmholtz free energies F_{sym}, F_{asym}, and F_{cap} of the symmetric, asymmetric, and capillary solutions, respectively, obtained with $\nu=1$ for the slit $\ell_w^*=15$ at $T=87$ K. The free energies are given for several average densities in the range of $\rho_{sb1}^* \leq \rho_{au}^* \leq \rho_{sb2}^*$ in units of k_BT/σ_{ff}^2.

	F_{sym}		F_{asym}		F_{cap}
ρ_{av}^*	BR[a]	PW[b]	BR[a]	PW[b]	PW[b]
0.1546	−26.59	−26.62	−26.67	−26.70	
0.2319	−39.66	−39.69	−39.86	−39.88	−39.12
0.3092	−52.81	−52.85	−53.06	−53.08	−52.32
0.3865	−66.01	−66.04	−66.26	−66.29	−65.65
0.4638	−79.22	−79.28	−79.48	−79.51	−79.26

[a]Data taken from Ref. 1.
[b]Calculated in the present work.

$$U_{sf}(z) = U_{sf1}\left(z + \frac{\sigma_{sf}}{2}\right) + U_{sf2}\left(\ell_w - z + \frac{\sigma_{sf}}{2}\right), \tag{2.25}$$

i.e., locating a hard-wall repulsion at a distance $\sigma_{sf}/2$ from the substrate. In this case, the effective width is

$$\ell_w = L - \sigma_{sf}, \tag{2.26}$$

as it is shown in Fig. 2 of Ref. 38.

In Fig. 1 we compare the potentials outlined in the previous paragraph. The comparison is restricted to the region close to the substrate. The quantity ξ is the perpendicular distance from the real wall being

$$\xi = \begin{cases} z + \sigma_{sf} & \text{for Berim – Ruckenstein} \\ z + \sigma_{sf}/2 & \text{for Nilson – Griffiths.} \end{cases} \tag{2.27}$$

One may realize that Eq. (2.25) retains the "soft" repulsion $[U_{sf}(z) \propto (\sigma_{sf}/z)^9]$, while Eq. (2.23) cuts the potential before the minimum be reached. This feature produces important effects on the behavior of the density profiles. In fact, the calculations performed by Berim and Ruckenstein[1] yielded density profiles with $\rho(z=0)$ and $\rho(z=\ell_w)$ different from zero, indicating that the fluid is in contact with the hard walls, while in the case of Nilson and Griffiths[38] the fluid forms a well defined first layer separated from the wall.

In the present work we shall analyze the evolution of asymmetric solutions when the total adsorption potential is written as

$$U_{sf}(z) = U_{sf1}\left(z + \frac{\sigma_{sf}}{\nu}\right) + U_{sf2}\left(\ell_w - z + \frac{\sigma_{sf}}{\nu}\right), \tag{2.28}$$

and the parameter ν varies from 1 to 2. In doing so, one goes from Eq. (2.23) toward Eq. (2.25) increasing the strength of the solid-fluid attraction.

III. NUMERICAL RESULTS AND DISCUSSION

Let us now describe the obtained results. The EL Eq. (2.14) was solved at fixed ℓ_w and T for a given number of particles per unit area N_s. The latter quantity determines an average fluid density $\rho_{av}=N_s/\ell_w$. A widely used computational algorithm consisting of a numerical iteration of the coupled Eqs. (2.17)–(2.19) was applied. This procedure yields the density profile $\rho(z)$ and the value of the Lagrange multiplier μ. The convergence of the solutions are measured by the difference between two consecutive profiles,

$$\delta_1 = \sigma_{ff}^5 \int_0^{\ell_w} dz[\rho_{i+1}(z) - \rho_i(z)]^2, \tag{3.1}$$

where $\rho_i(z)$ is the density profile after the ith iteration, and by the quantity

$$\delta_2 = 1 - \frac{1}{N_s}\int_0^{\ell_w} dz\rho(z), \tag{3.2}$$

accounting for the deviation from the required N_s.

In practice, for the calculations it is convenient to use dimensionless variables: $z^*=z/\sigma_{ff}$ for the distance, $\rho^*=\rho\sigma_{ff}^3$ for the densities, and $T^*=k_BT/\varepsilon_{ff}$ for the temperature. In these units the average density becomes $\rho_{av}^*=N_s\sigma_{ff}^2/\ell_w^*=N_s^*/\ell_w^*$. For the numerical task, the region of integration $[0,\ell_w^*]$ was divided into a grid of equal intervals $\Delta z^*=0.02$, i.e., a grid with 50 points per atomic diameter σ_{ff}. It is worthwhile to notice that in the work of Berim and Ruckenstein the number of grid points was taken equal to 10 per atomic diameters. If the obtained profile did not change with increasing precision from $\delta_1 \approx 10^{-8}$ to $\delta_1 \approx 10^{-15}$, then it was accepted as a solution of the coupled integral equations.

In a first step, we studied the same systems treated in detail by Berim and Ruckenstein.[1] Hence, we set $\nu=1$ and solved the EL equation for a slit with an effective width $\ell_w^*=15$ at $T=87$ K ($T^*=0.73$) for a series of average fluid density $\rho_{av}^*=N_s^*/\ell_w^*$. The ground state solutions yield symmetric density profiles for $\rho_{av}^* < 0.1=\rho_{sb1}^*$ and for $\rho_{av}^* > 0.514=\rho_{sb2}^*$, while in the range of $\rho_{sb1}^* \leq \rho_{av}^* \leq \rho_{sb2}^*$ the ground state solutions provide asymmetric density profiles. This is due to the fact that in such a regime the asymmetric solutions have lower free energy than the symmetric ones. The free energies calculated for some selected ρ_{av}^* are listed in Table I together with the results obtained by Berim and Ruckenstein.[1] A glance at this table indicates a good agreement between both sets of values. In order to get symmetric solutions in the range of $0.1 \leq \rho_{av}^* \leq 0.513$, one must explicitly impose such a condition to Eqs. (2.17)–(2.19).

The Lagrange multiplier μ (equivalent to the chemical potential in the case of open slits) is displayed in Fig. 2 as a function of average density. We show the results for a wider range of ρ_{av}^* than it is done in Fig. 9 of Ref. 1. Figure 2 clearly indicates that the asymmetric solutions occur in the domain where μ is degenerate, namely, the same value of μ corresponds to different ρ_{av}^*. That is just the regime where in

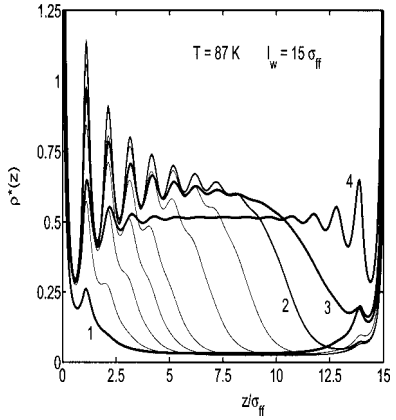

FIG. 4. Asymmetric density profiles as a function of the distance from the hard-wall repulsion. It is shown the evolution for increasing density average at $\nu=1$. Data for $\rho^*_{av}=0.1063$, 0.1159, 0.1546, 0.1932, 0.2319, 0.3092, 0.3892, 0.4638, 0.5135, and 0.5139 are displayed. These values cover the whole range $\rho^*_{sb1} \leqslant \rho^*_{av} \leqslant \rho^*_{sb2}$ where there are asymmetric solutions.

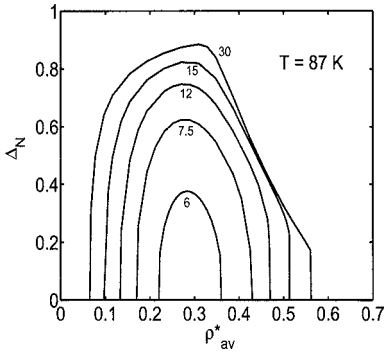

FIG. 5. Asymmetry parameter defined in Eq. (2.20) as a function of average density. The successive curves are results obtained for slits with different effective widths labeled by ℓ^*_w. For each width the asymmetric solutions occur in different ranges $\rho^*_{sb1} \leqslant \rho^*_{av} \leqslant \rho^*_{sb2}$.

the case of an open slit the equal-area Maxwell construction should be applied in order to determine the chemical potential (cf., e.g., Fig. 2 in Ref. 36). In addition, it is worthwhile to notice that at ρ^*_{sb2} there is an abrupt jump of μ, we shall come back to this feature below.

If one manages conveniently the EL equation it is possible to get another kind of symmetric solutions in some region of ρ^*_{av}. The free energy of such new solutions is included in Table I and the corresponding multiplier μ is plotted in Fig. 2. Figure 3 shows the special distribution of all three states listed in Table I for $\rho^*_{av}=0.3865$. A direct comparison indicates that these three profiles correspond to the *drying*, the *one-wall wetting*, and the *two-wall wetting* cases displayed, respectively, in Figs. 1–3 of Ref. 28. From a glance at Table I one realizes that as long as the film wetting solution exists the drying one is a symmetric excited state. In the regime $\rho^*_{av} > \rho^*_{sb2}$ the drying profile shown in Fig. 3 becomes the capillary condensation (CC) solution.

Figure 4 shows a series of asymmetric density profiles $\rho^*(z)=\rho(z)\sigma^3_{ff}$. This sequence indicates that for increasing average density, starting from the profile denoted as 1 ($\rho^*_{av}=0.1063$), the number of oscillations near the left wall as well as its amplitudes increase. This trend continues up to the profile 2 ($\rho^*_{av}=0.4638$), where the peaks of the oscillating structure begin to decrease. Furthermore, profile 3 corresponds to the biggest asymmetric solution, for larger ρ^*_{av} there is a jump to the symmetric profile 4. The latter behavior indicates a transition to the so-called CC phase, i.e., a transition to a situation where the slit is full of liquid argon. The jump of μ addressed in the previous paragraph is also a manifestation of this thick film to CC transition.

The asymmetry of the profiles for $\nu=1$ displayed in Fig. 4 was measured by the parameter Δ_N introduced in Eq. (2.20). The results are shown in Fig. 5. These values are essentially the same as that of the equivalent curve displayed in Fig. 5 of Ref. 1. As mentioned in the Introduction, in Refs. 25–28, 30, and 31, it is emphasized that a slit of width $\ell^*_w=30$ is appropriate to study wetting because it is large enough to avoid any confinement effect. Therefore, it becomes of interest to solve the EL equation for such a big slit and to compare the results with that obtained for $\ell^*_w=15$. The asymmetry parameter evaluated for the $\ell^*_w=30$ slit at $T=87$ K is also plotted in Fig. 5. A comparison of the curves labeled by 30 and 15 indicates that its shapes do not differ significantly, in particular, in the regime of large coverage $0.35 \leqslant \rho^*_{av} \leqslant 0.51$ the values of Δ_N are almost equal. Hence, we can state that the capillary effects in the case of the moderately thick slit of $\ell^*_w=15$ are not very important.

For the sake of completeness we also analyzed slits of $\ell^*_w<15$ at $T=87$ K. The asymmetry parameters evaluated for $\ell^*_w=12$, 7.5, and 6 are included in Fig. 5. It is clear that these curves exhibit everywhere an increasing departure from the $\ell^*_w=30$ results. Finally, for $\ell^*_w=5.5$ the parameter Δ_N becomes zero for all ρ^*_{av}, indicating that the asymmetric solution disappears.

In the next step, we analyzed the change of the properties described above when the parameter ν is taken larger than unity. The variation of ν is performed in such a way that the effective width of the slit is always kept at $\ell^*_w=15$, hence, only the potential is slightly changed mainly near the walls. At this point the temperature was still kept at $T=87$ K. It was found that for increasing values of ν the range of average density $\rho^*_{sb1} \leqslant \rho^*_{av} \leqslant \rho^*_{sb2}$ where there are symmetry breaking decreases. This effect might be observed in successive plots of μ versus ρ^*_{av}, however, we prefer to report directly the evolution of the parameter Δ_N. Figure 6 shows how this parameter decreases with increasing ν. From this figure one may conclude that symmetry breaking persists at most for $\rho^*_{av} \approx 0.2$.

Figure 7 shows the asymmetry parameter Δ_N as a function of the factor ν for the average density $\rho^*_{av}=0.1932$. These data indicate that the asymmetric solution already disappears for a critical value $\nu_c \simeq 1.18$. The evolution of the density profiles from asymmetric to symmetric species is displayed in Fig. 8. In this drawing one may observe the diffusion of fluid argon from the neighborhood of the left wall toward the right one. This process continues until a symmetric density profile is formed for $\nu \simeq 1.2$. The described evolution of $\rho^*(z)$ is determined by the behavior of the surface tensions. If one uses Young's law given in Eq. (1.1) the total surface excess energy of asymmetric profiles may be written as

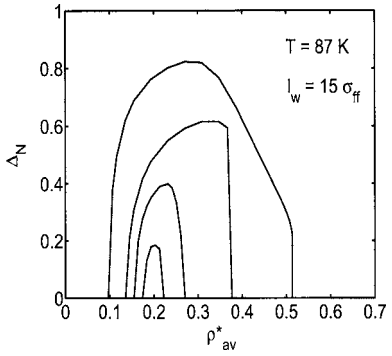

FIG. 6. Asymmetry parameter of density profiles, defined in Eq. (2.20), as a function of average density. Going from the outer curve toward the inner one the data correspond, respectively, to $\nu=1$, 1.136, 1.156, and 1.170. If $\nu>1.18$ for all ρ_{av}^{*} one gets $\Delta_N=0$.

$$\gamma_{\mathrm{tot}}=\gamma_{\mathrm{SL}}+\gamma_{\mathrm{LV}}+\gamma_{\mathrm{SV}}=2\gamma_{\mathrm{SL}}+\gamma_{\mathrm{LV}}(1+\cos\theta), \tag{3.3}$$

with $\cos\theta=(\gamma_{\mathrm{SV}}-\gamma_{\mathrm{SL}})/\gamma_{\mathrm{LV}}<1$. By increasing enough the attraction the equality $\gamma_{\mathrm{SV}}-\gamma_{\mathrm{SL}}=\gamma_{\mathrm{LV}}$ is reached yielding $\cos\theta=1$, then the system undergoes to a transition to a symmetric profile with

$$\gamma_{\mathrm{tot}}=2\gamma_{\mathrm{SL}}+2\gamma_{\mathrm{LV}}. \tag{3.4}$$

In this case both walls of the slit are wet.

Let us now look if something special is going on for the adsorption potential at $\nu_c\simeq 1.18$. As a matter of fact, it becomes important to explore where the hard-wall repulsion introduced in Ref. 1 is located for such a critical value. The position of the left hard-wall repulsion with respect to the real wall according to Fig. 1 is given by

$$\xi_{\mathrm{HW}}^{c}=\frac{\sigma_{sf}}{\nu_c}. \tag{3.5}$$

For a slit of effective width $\ell_w^{*}=15$ the minimum of the total adsorption potential given by Eq. (2.25) is to a very good approximation determined by the minimum of the ES potential exerted by the left wall. It is located at

$$\xi_{\mathrm{min}}=\left(\frac{2}{5}\right)^{1/6}\sigma_{sf}. \tag{3.6}$$

The ratio of these quantities becomes

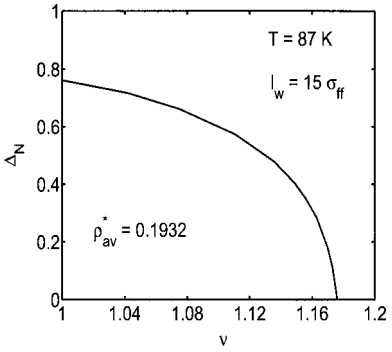

FIG. 7. Asymmetry parameter of density profiles, defined in Eq. (2.20), obtained for the average density $\rho_{\mathrm{av}}^{*}=0.1932$ as a function of the factor ν.

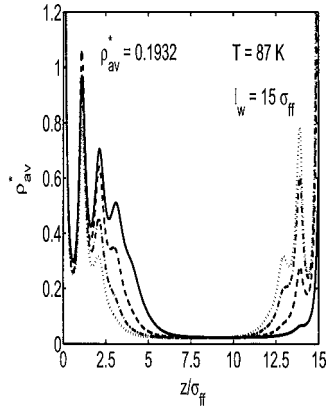

FIG. 8. Evolution of the asymmetric solution for the average density $\rho_{\mathrm{av}}^{*}=0.1932$ in terms of the factor ν. The solid curve corresponds to $\nu=1$, the dashed to 1.136, the dashed-dotted to 1.156, and the dotted to 1.2.

$$\frac{\xi_{\mathrm{min}}}{\xi_{\mathrm{HW}}^{c}}=\left(\frac{2}{5}\right)^{1/6}\nu_c\simeq 1.013. \tag{3.7}$$

Since this ratio is larger than unity, it indicates that for ν_c the minimum of the ES potential is reached inside the slit.

We also analyzed the occurrence of asymmetric solutions for $1\leqslant\nu<2$ at temperatures $T>87$ K. It was also found that the symmetry breaking disappears at some critical value of ν. Such a behavior may be expected if one takes into account that for temperatures larger than $T=87$ K even for $\nu=1$ the range $\rho_{\mathrm{sb1}}\leqslant\rho_{\mathrm{av}}\leqslant\rho_{\mathrm{sb2}}$ is smaller (see Fig. 5 of Ref. 1).

It is worthwhile to notice that a reliable *ab initio* potential utilized by Mistura *et al.*[22] for investigating the adsorption of Ar on CO_2 exhibits an even stronger attraction than the ES potential. This feature can be observed in Fig. 3 of Ref. 22. Hence, one would not expect any symmetry breaking in the case of such a realistic adsorption potential.

IV. FINAL REMARKS

We reexamined the symmetry breaking found very recently by Berim and Ruckenstein[1] in a study of the adsorption of argon in a closed slit with identical walls of carbon dioxide. It is important to stress that these authors have introduced hard-wall repulsions at distances $d_{\mathrm{BR}}=\sigma_{sf}$ from the real walls of the slit, as shown in Fig. 1 (see also Fig. 2 in Ref. 1), reducing in such a way the strength of the adopted ES potential. Stable asymmetric solutions were obtained in the case of a slit with effective width $\ell_w^{*}=15$ for temperatures in the range of $87\leqslant T\leqslant 106$ K.

The present study was mainly devoted to establish how robust are the asymmetric solutions against changes of the adsorption potential. However, in addition, the behavior of the asymmetry parameter was also evaluated for slits of different widths. The calculations have been carried out using the same nonlocal formalism as that adopted in Ref. 1, namely, the SDA DFT proposed by Tarazona.[2]

Since in a pioneering series of works a Dutch Collaboration have previously found the symmetry breaking by studying adsorption in a slit of width $\ell_w^{*}=30$, see Refs. 25–28, we performed a comparison of the asymmetry param-

eter Δ_N evaluated for slits of $\ell_w^*=15$ and 30 at $T=87$ K. The difference between the results is rather small. Further calculations showed that the effect due to confinement begins to be important for slits with $\ell_w^* \leqslant 12$.

Focusing the analysis on the slit of $\ell_w^*=15$, in a rather complete plot of μ versus ρ_{av}^*, we show clearly the regime where the symmetry breaking occurs and, in addition, we also display the Lagrange multiplier μ for a CC-like solution. Furthermore, it is shown that the spacial shape of the obtained solutions correspond to the three sorts of profiles discussed in Refs. 25–28. The strength of the attraction determines which one of that profiles is the stable solution.

By shifting the hard-wall repulsions introduced by Berim and Ruckenstein[1] toward the real walls the strength of the attraction is increased producing changes in the balance of surface tensions. It was found that at $T=87$ K already for the critical distance $d_c \simeq d_{\mathrm{BR}}/1.2$ the asymmetric solutions disappear. At this temperature, close to the triple point, the asymmetry parameter Δ_N reached its largest values in the study of Ref. 1. For higher temperatures the symmetry breaking disappears even more rapidly.

Finally, we can state that from the present study it is possible to conclude that the symmetry breaking reported in Ref. 1 can be understood in terms of findings described in Refs. 25–28. By locating hard-wall repulsions the authors of Ref. 1 diminish the attraction of the ES adsorption potential exerted on the fluid causing the entrance of the system in a *one-wall-wetting* regime (asymmetric profiles) corresponding to Fig. 2 of Ref. 28. By moving the hard-wall repulsions toward the real walls the attraction increases monotonically causing eventually the entrance of the system in the *two-wall wetting* regime with symmetric solution of the type displayed in Fig. 3 of Ref. 28.

Furthermore, a reliable *ab initio* potential for the interaction of fluid Ar with a structureless smooth wall of CO_2 like that adopted by Mistura *et al.*[22] is even stronger than the ES one. Therefore, it is possible to infer that no symmetry breaking would be expected for real Ar/CO_2 systems.

ACKNOWLEDGMENTS

This work was supported in part by the Ministry of Culture and Education of Argentina through Grants CONICET PIP No. 5138/05, ANPCyT BID 1728/OC-PICT No. 31980, and UBACYT No. X298.

[1] G. O. Berim and E. Ruckenstein, J. Chem. Phys. **126**, 124503 (2007).
[2] P. Tarazona, Phys. Rev. A **31**, 2672 (1985); *ibid.* **32**, E3148 (1985).
[3] P. Tarazona, U. M. B. Marconi, and R. Evans, Mol. Phys. **60**, 573 (1987).
[4] D. Nicholson and N. G. Parsonage, *Computer Simulation and the Statistical Mechanics of Adsorption* (Academic, London, 1982), Chap. 7.
[5] L. W. Bruch, M. W. Cole, and E. Zaremba, *Physical Adsorption* (Oxford University Press, Oxford, 1997).
[6] C. Ebner and W. F. Saam, Phys. Rev. Lett. **38**, 1486 (1977); W. F. Saam and C. Ebner, Phys. Rev. A **17**, 1768 (1978).
[7] D. E. Sullivan, Phys. Rev. B **20**, 3991 (1979).
[8] M. J. Johnson and S. Nordholm, J. Chem. Phys. **75**, 1953 (1981).
[9] S. M. Foiles and N. W. Ashcroft, Phys. Rev. B **25**, 1366 (1982).
[10] P. Tarazona and R. Evans, Mol. Phys. **47**, 1033 (1982); Mol. Phys. **48**, 799 (1983).
[11] R. Evans and P. Tarazona, Phys. Rev. A **28**, 1864 (1983).
[12] T. F. Meister and D. M. Kroll, Phys. Rev. A **31**, 4055 (1985).
[13] E. Bruno, C. Caccamo, and P. Tarazona, Phys. Rev. A **34**, 2513 (1987); Phys. Rev. A **35**, 1210 (1987).
[14] J. E. Finn and P. A. Monson, Phys. Rev. A **39**, 6402 (1989).
[15] S. Sokolowski and J. Fischer, Phys. Rev. A **41**, 6866 (1990).
[16] E. Velasco and P. Tarazona, Phys. Rev. A **42**, 2454 (1990).
[17] J. E. Finn and P. A. Monson, Phys. Rev. A **42**, 2458 (1990).
[18] Y. Fan and P. A. Monson, J. Chem. Phys. **99**, 6897 (1993).
[19] Y. Fan, J. E. Finn, and P. A. Monson, J. Chem. Phys. **99**, 8238 (1993).
[20] E. Kierlik, M. L. Rosinberg, Y. Fan, and P. A. Monson, J. Chem. Phys. **101**, 10947 (1994).
[21] E. Kierlik, Y. Fan, P. A. Monson, and M. L. Rosinberg, J. Chem. Phys. **102**, 3712 (1995).
[22] G. Mistura, F. Ancilotto, L. Bruschi, and F. Toigo, Phys. Rev. Lett. **82**, 795 (1999).
[23] A. F. Bakker, thesis, Technische Universiteit Delft, 1983.
[24] A. F. Bakker and C. Bruin, in *Special Purpose Computers*, edited by B. J. Alder (Academic, London, 1988).
[25] J. H. Sikkenk, J. O. Indekeu, J. M. J. van Leeuwen, and E. O. Vossnack, Phys. Rev. Lett. **59**, 98 (1987).
[26] J. H. Sikkenk, J. O. Indekeu, J. M. J. van Leeuwen, E. O. Vossnack, and A. F. Bakker, J. Stat. Phys. **52**, 23 (1988).
[27] M. J. P. Nijmeijer, C. Bruin, A. F. Bakker, and J. M. J. van Leeuwen, Physica A **160**, 166 (1989).
[28] M. J. P. Nijmeijer, C. Bruin, A. F. Bakker, and J. M. J. van Leeuwen, Phys. Rev. A **42**, 6052 (1990).
[29] P. G. de Gennes, Rev. Mod. Phys. **57**, 827 (1985).
[30] E. Velasco and P. Tarazona, J. Chem. Phys. **91**, 7916 (1989).
[31] J. R. Henderson, P. Tarazona, F. van Swol, and E. Velasco, J. Chem. Phys. **96**, 4633 (1992).
[32] P. I. Ravikovitch, A. Vishnyakov, and A. V. Neimark, Phys. Rev. E **64**, 011602 (2001).
[33] J. K. Percus and G. J. Yevick, Phys. Rev. **110**, 1 (1958).
[34] N. F. Carnahan and K. E. Starling, J. Chem. Phys. **51**, 635 (1969); Phys. Rev. A **1**, 1672 (1970).
[35] J. A. Barker and D. Henderson, Rev. Mod. Phys. **48**, 587 (1976).
[36] F. Ancilotto and F. Toigo, Phys. Rev. B **60**, 9019 (1999).
[37] P. J. Marshall, M. M. Szczęśniak, J. Sadlej, G. Chalasiński, M. A. ter Horst, and C. J. Jameson, J. Chem. Phys. **104**, 6569 (1996).
[38] R. H. Nilson and S. K. Griffiths, J. Chem. Phys. **111**, 4281 (1999).